

RESEARCH ARTICLE | MAY 28 2024

# Mapping the transition from quasi-2D to 3D spin textures in NiFe nanomagnets

J. R. Scott   ; D. Atkinson  ; A. O. Adeyeye  

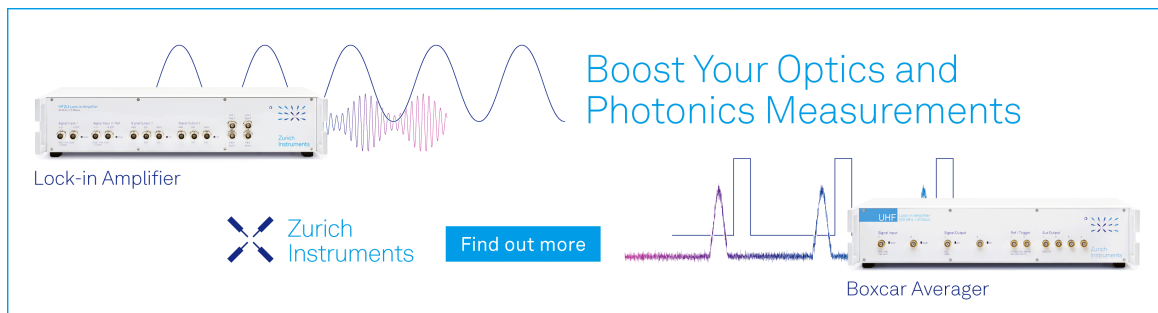
 Check for updates

*Appl. Phys. Lett.* 124, 222403 (2024)


<https://doi.org/10.1063/5.0212429>



Boost Your Optics and Photonics Measurements



Lock-in Amplifier



Find out more

Boxcar Averager

# Mapping the transition from quasi-2D to 3D spin textures in NiFe nanomagnets

Cite as: Appl. Phys. Lett. **124**, 222403 (2024); doi: [10.1063/5.0212429](https://doi.org/10.1063/5.0212429)

Submitted: 4 April 2024 · Accepted: 11 May 2024 ·

Published Online: 28 May 2024



View Online



Export Citation



CrossMark

J. R. Scott,<sup>a)</sup>  D. Atkinson,<sup>a)</sup>  and A. O. Adeyeye<sup>a)</sup> 

## AFFILIATIONS

Department of Physics, Durham University, Durham DH1 3LE, United Kingdom

<sup>a)</sup>Authors to whom correspondence should be addressed: [jay.r.scott@durham.ac.uk](mailto:jay.r.scott@durham.ac.uk) and [adekunle.o.adeyeye@durham.ac.uk](mailto:adekunle.o.adeyeye@durham.ac.uk)

## ABSTRACT

With increasing interest in understanding and mapping the spin textures within magnetic nanostructures, this work reports a study of the transition from quasi-2D magnetic behavior in thin-film ferromagnetic nanostructures to 3D thick-film nanostructures. A series of arrays of  $480 \times 250 \text{ nm}^2$  elliptical  $\text{Ni}_{81}\text{Fe}_{19}$  nanomagnets patterned using deep ultraviolet (DUV) lithography with thickness ( $t$ ) ranging from 20 to 250 nm were studied. It is shown through magnetometry and micromagnetics that as the film thickness increases, the nanomagnets transition from effectively planar 2D magnets, with uniform spin textures extending through the film thickness for  $t \leq 50 \text{ nm}$ , to 3D nanomagnets with more complex non-uniform 3D spin textures for  $t \geq 100 \text{ nm}$ . These results demonstrate that the fabrication of thick-film nanomagnets via DUV lithography is a viable route to producing consistent 3D magnetic nanostructures for potential applications, such as magnonics.

© 2024 Author(s). All article content, except where otherwise noted, is licensed under a Creative Commons Attribution-NonCommercial-NoDerivs 4.0 International (CC BY-NC-ND) license (<https://creativecommons.org/licenses/by-nc-nd/4.0/>). <https://doi.org/10.1063/5.0212429>

The field of nanomagnetism has expanded hugely over the past two decades, with work on magnetic nanostructures directed to a range of technologies, from memory and sensors to logical processing applications,<sup>1–5</sup> and most recently, magnonics<sup>6</sup> and neuromorphic computing.<sup>7</sup> Underpinning these advances is an understanding of the magnetization distributions and reversal processes within these systems, which is critical for realizing their functional performance. With device applications in mind, research activity has often focused on well-defined lithographically patterned thin-film nanostructures in which the magnetization through the thickness is uniform, so the layer is effectively 2D.<sup>8,9</sup> The magnetization structure is determined largely by rotational, vortex,<sup>10–12</sup> and domain wall magnetization processes.<sup>13–16</sup> More recently, there has been a critical expansion of research into 3D magnetic nanostructures associated with developments in both fabrication methods and with imaging and analysis of the 3D magnetization that occurs within these complex magnetic objects.<sup>17–19</sup> 3D structures based on 2-photon lithography,<sup>20</sup> scaffolds, or direct write growth<sup>21</sup> among others are enabling the study of complex 3D spin structures that may have potential for future applications, although the fabrication of such complex 3D structures is currently specialized and relatively slow.

Deep ultraviolet (DUV) lithography is a well-established industrial process for rapid, large-area, high-resolution nanofabrication, which is ubiquitous in today's semiconductor industry. DUV

lithography can be used to pattern thick layers of resist, enabling the fabrication of high-quality 3D nanostructures or nanomagnets (NMs), where the thicknesses are comparable with the planar feature sizes. In contrast, electron-beam lithography, another lithography technique commonly used by researchers in this field, typically requires the use of thinner resist layers.<sup>22</sup>

Here, we have used DUV lithography to pattern large areas of high-quality NMs in which the film thickness was varied to investigate the magnetization structures and reversal behavior through the transition from quasi-2D to 3D magnetic nanostructures. A combination of experimental magnetization measurements and micromagnetic simulations were used to study a system composed of elliptical NMs.

The experimental system consists of an array of elliptical NMs with dimensions  $480 \times 250 \text{ nm}^2$ . The NMs are spaced sufficiently far apart that magnetostatic interactions between them are considered negligible, and each NM is effectively isolated (see the [supplementary material](#) for more details). Arrays of magnetic nanostructures were fabricated over a large area ( $4 \times 4 \text{ mm}^2$ ) on silicon substrates using deep UV lithography at an exposure wavelength of 193 nm. The nanostructures were fabricated by deposition and liftoff of a layer of  $\text{Ni}_{81}\text{Fe}_{19}$  Permalloy (Py), with a thickness ( $t$ ) ranging from 20 to 250 nm, using thermal evaporation from a single source at a growth rate of  $0.8 \text{ \AA/s}$  from a base pressure of  $1.9 \times 10^{-5} \text{ Pa}$ . Ultrasonic liftoff with OK73 resist-thinner was used for the removal of the photoresist.

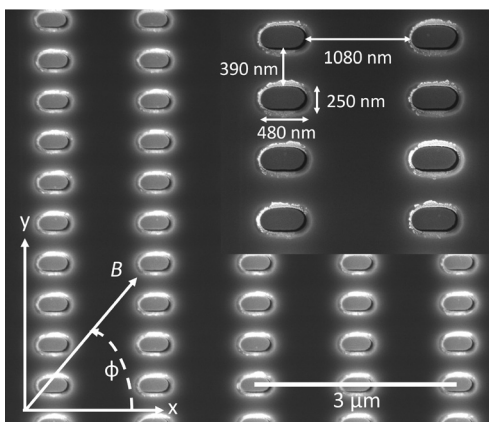
The completion of the liftoff process was verified using scanning electron microscopy (SEM).

The magnetization reversal processes were measured using a vibrating sample magnetometer (VSM) with the applied field ( $B$ ) in-plane and directed either along the long or short axes of the NMs.

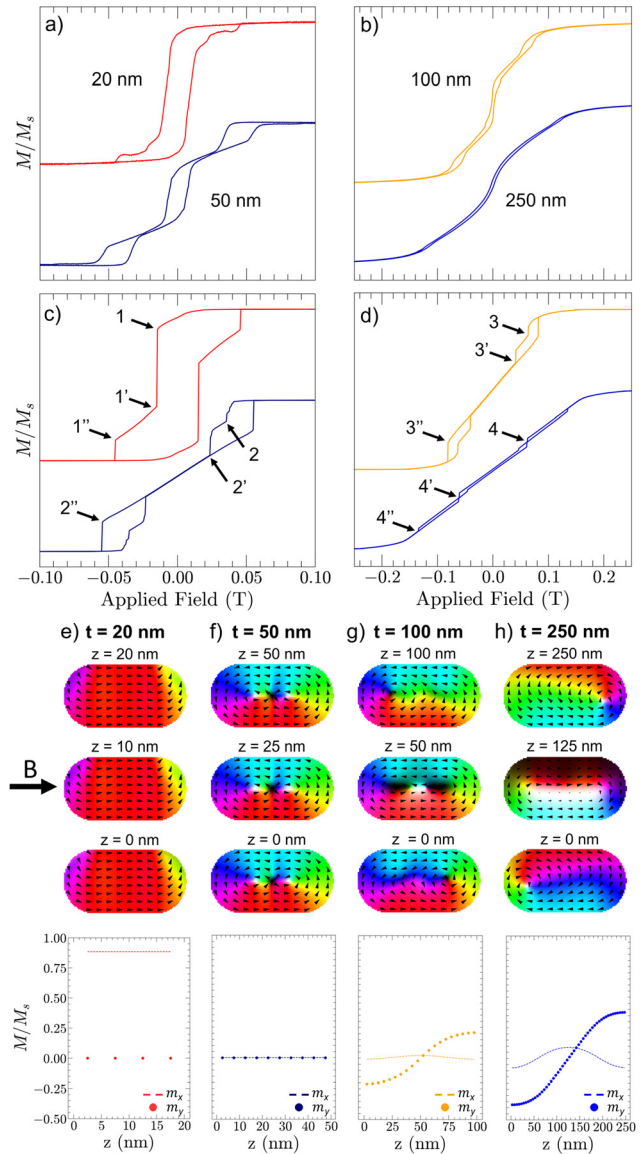
Micromagnetic simulations were undertaken using the GPU-based Mumax3 software.<sup>23</sup> The dimensions of the NMs and the spacing between them were extracted from the SEM images. In order to optimize the simulation time, only a single element was simulated, which assumes that the magnetostatic coupling between elements is negligible, as it is for the experimental NMs. This is a reasonable assumption given that the spacing between neighboring NMs is much larger than their lateral dimensions. The samples were also considered to be uniform, with no inclusion of defects, pinning sites, or finite temperature effects. Standard input parameters for micromagnetic simulations of Py were used: exchange stiffness constant  $A = 1.30 \times 10^{-11}$  J/m, saturation magnetization  $M_s = 8.6 \times 10^5$  A/m, zero magnetocrystalline anisotropy ( $K_u$ ), and gyromagnetic ratio  $\gamma/2\pi = 28$  GHz/T. The micromagnetic cell size was  $(5 \text{ nm})^3$ , consistent with the common estimate for the exchange length in Py, and the system was initialized with a random magnetization state to solve the Landau–Lifshitz–Gilbert (LLG) equation.

Figure 1 shows an SEM image of a typical array of NMs, with an inset showing the key dimensions. The image shows that the NMs are uniform over large areas, with bright contrast indicating remnants of resist around some nanostructures.

The magnetic hysteresis of the arrays of NMs measured along the  $\phi = 0$  direction are shown in Figs. 2(a) and 2(b) for a series of film thicknesses from 20 nm up to 250 nm. For the 20 nm thick structures, the magnetization reversal is dominated by a large switching event at  $B \leq 20$  mT, followed by a region of smaller magnetization changes extending to saturation. This suggests the uniform reversal of a large axial component of the magnetization followed by the alignment of some spin texture that is likely to form at the ends of the NM long axis to reduce the magnetostatic energy, and/or the sharp feature at the end of the tail could indicate the annihilation of a vortex core. For the



**FIG. 1.** SEM image of an array of widely spaced Permalloy nanomagnets. The inset panel details the dimensions of the elliptical nanomagnets and their spacing. The axes in the bottom left show the coordinate system used for the hysteresis measurements, with  $\phi = 0^\circ$  ( $\phi = 90^\circ$ ) corresponding to an applied magnetic field  $B$  along the long (short) axis of the nanomagnets.



**FIG. 2.** (a) VSM measurements performed on the  $t = 20$  nm and  $t = 50$  nm films, with the magnetic field applied along the  $\phi = 0^\circ$  direction; and the corresponding results of micromagnetic simulations are shown in (c). (b) VSM measurements performed on the  $t = 100$  and 250 nm films with  $\phi = 0^\circ$ , with the corresponding simulation results shown in (d). (e)–(h) Simulated remanent magnetization states of the top, middle, and bottom layers in the  $xy$  plane for the  $t = 20, 50, 100,$  and 250 nm films, respectively, with the panels at the bottom showing the corresponding normalized in-plane magnetization components  $m_x$  and  $m_y$  as a function of the  $z$ -position.

50 nm thick NMs, the reversal in the hysteresis shows three sharp steps separated by sections with continuous magnetization changes. The initial and final steps in the magnetization reversal may be associated with vortex nucleation and annihilation, comparable to early work on circular NMs of similar dimensions and thickness;<sup>8</sup> however, here, the magnetization at low fields has a significant axial component in

addition to the vortex contribution to the magnetization state. When the film thickness is 100 nm, the hysteresis shows similar steps combining vortex-like and axial magnetization components, but over a larger field range [note the different  $x$ -axis scale between Figs. 2(a) and 2(b)]. For the thickest film of 250 nm, the in-plane NM dimensions are comparable with the NM thickness, and, in this case, the in-plane magnetization behavior shows reversal of the magnetization with little hysteresis, but again with a region of steeper reversal at low fields and small features at higher fields prior to saturation.

Micromagnetic simulations of the magnetization reversal for the equivalent Py NMs are presented in Figs. 2(c) and 2(d). For the 20 nm thick NM, the micromagnetic simulations show that the magnetization reversal occurs via the switching of a large axial component of magnetization accompanied by the nucleation of a vortex. This is then followed by a region of vortex squeezing toward the longer edge of the NM until it is annihilated and the reverse saturation state is reached. The overall hysteresis is generally consistent with the shape of the experimental results, with comparable field values and some difference in the relative size of the axial switching component. For the 50 nm thick NMs, there are two steps in the nucleation of a multi-vortex state followed by a more gradual squeezing of the vortices toward the longer edge of the NM until it is annihilated and the reverse saturation state is reached. This is comparable with the measured experimental behavior in terms of the nucleation and annihilation fields, but the details of the net magnetization after nucleation of the vortex state are different, with the experimental results showing the reversal of an axial component at low fields rather than just vortex squeezing. The micromagnetic simulations of the magnetization, through the reversal, show the nucleation, distortion, and annihilation of a vortex spin texture, as indicated by the selected simulated spin texture images in Fig. 3. The simulated magnetization reversal of the 100 nm thick NM is comparable with the experimental measurement, showing very little hysteresis and sharp features that the magnetization simulations show are associated with the nucleation and annihilation of multi-vortex spin textures. However, as for the 20 and 50 nm thick NMs, the experimental hysteresis measurement of the 100 nm thick NMs shows a more abrupt reversal of the magnetization close to zero field than the simulations. The magnetization simulations show that the nucleation of a multi-vortex state occurs at a negative field, and this state is annihilated at a

positive field of similar magnitude. For the 250 nm thick NM, there is almost anhysteretic linear magnetization reversal, with small hysteretic features at high fields and around zero field, indicating the onset of more complex spin textures that evolves as the magnetic field changes. The experimentally observed reversal is similar to the micromagnetic simulation showing very little hysteresis, but as for the other thicknesses, the rate of change of magnetization at low fields is larger in the VSM measurements than the simulations. Each of the reversal processes are further illustrated in Fig. 3 with each state being labeled according to the arrows in Figs. 2(c) and 2(d). In each case, only the slice through the middle of the thickness of the NM is shown; however, it is observed that the spin texture of the NMs becomes increasingly non-uniform as the thickness increases as shown in Fig. 2(e).

Overall, for the 20 nm thick NM, the spin texture is uniform throughout the film thickness, while for the 50 nm thick NM, only a slight rotation of the vortex core is observed. This uniformity is further illustrated in the bottom panels of Figs. 2(e) and 2(f) where  $m_x$  and  $m_y$  remain constant with changing  $z$ -position. In the 100 nm thick NM, the spin texture varies significantly through the thickness, with a vortex core shifted left and right of the center in the top and bottom layers, respectively, and domains with strong out-of-plane components present in the middle layer. These vortices grow in size through the layers toward the middle layer, where both vortices are present within a region where the magnetization undergoes a helical rotation between the vortex cores. For the 250 nm thick NM, the spin texture has a vortex core shifted left from the center in the bottom layer. The vortex core grows toward the right-hand side of the NM as  $z$  increases, until it extends across most of the long axis in the middle layer of the NM. The vortex core then shrinks as the domain on the left-hand side grows until the top layer is reached, and the vortex core resides on the opposite side of the NM compared to the bottom layer. The bottom panels of Figs. 2(g) and 2(h) further show how the  $y$ -component of magnetization reverses as the vortex cores shift between the top and bottom layers of the 100 and 250 nm thick NMs.

Magnetic hysteresis was also measured with the magnetic field applied along the  $\phi = 90^\circ$  direction, i.e., along the short axis of the NMs. Figure 4 shows the experimental and simulated magnetic hysteresis loops. Comparing with the results obtained along the  $\phi = 0^\circ$ , the most noticeable change to the hysteresis loop occurs for the 20 nm thick NM where the reversal involves the nucleation of a vortex spin texture, which is present at remanence as shown in Fig. 4(e). There is agreement between the micromagnetic and experimentally measured hysteresis in the presence of features at high fields, but, similar to the comparison along the  $\phi = 0^\circ$  axis, the experimental measurements show larger, hysteretic magnetization changes at low fields. For the thicker NMs, the results are quite similar to those obtained for  $\phi = 0^\circ$ .

The trends in the simulated remanent magnetization states are the same as seen for  $\phi = 0^\circ$ : as the thickness increases, the spin texture becomes increasingly non-uniform through the thickness and becomes increasingly out-of-plane (OOP) in the interior of the NMs. As discussed earlier, the 20 nm thick NM with  $\phi = 90^\circ$  has a vortex spin texture, which is uniform through the film thickness, and this is also the case for  $t = 50$  nm. Interestingly, the remanent state for the 100 nm thick NM has largely the same spin texture in the  $xy$  plane as the 250 nm thick NM with  $\phi = 0^\circ$ , albeit with the vortex core being of opposite polarity. This is further illustrated by the bottom panels of Figs. 4(g) and 2(g) being inverted with respect to each other. The remanent state of the 250 nm thick NM with  $\phi = 90^\circ$  is unique.

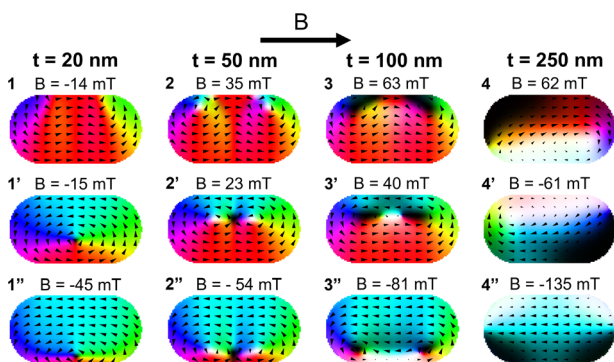


**FIG. 3.** Simulated magnetization states at three different stages of the reversal process labeled according to the arrows in Figs. 2(c) and 2(d), with only the slice through the middle layer shown in each case. The black and white contrast indicates out-of-plane magnetization components.



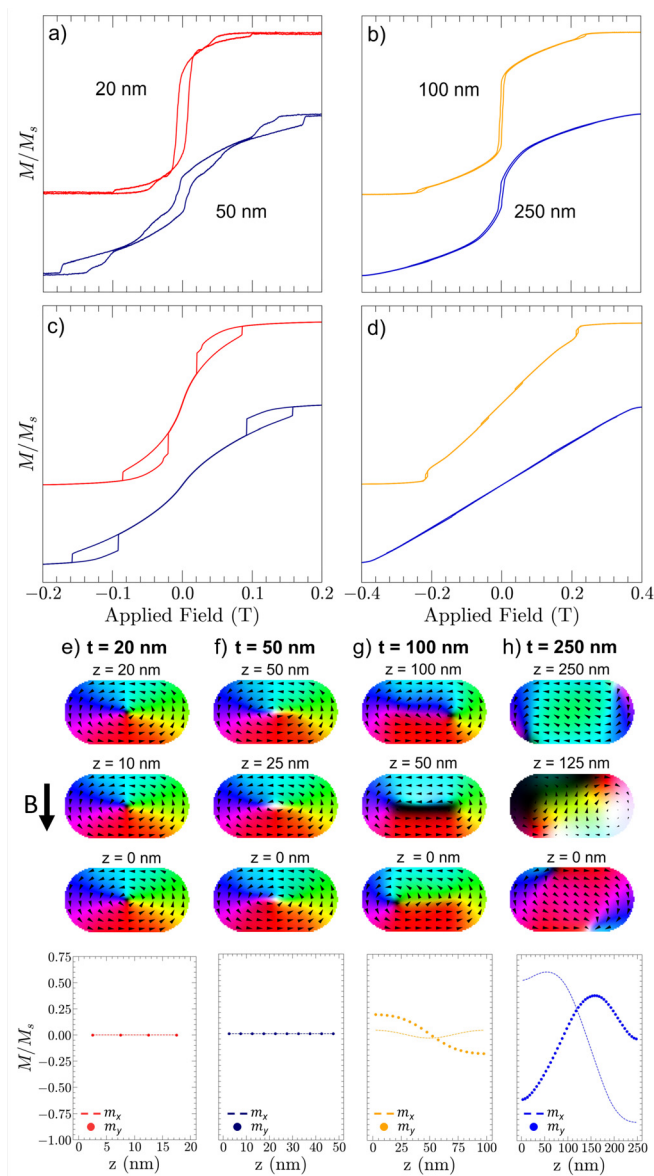


**FIG. 4.** VSM measurements performed on the  $t = 20$  nm and  $t = 50$  nm films with the magnetic field applied along the  $\phi = 90^\circ$  direction, and the corresponding results of micromagnetic simulations are shown in (c). (b) VSM measurements performed on the  $t = 100$  and  $250$  nm films with  $\phi = 90^\circ$ , with the corresponding simulation results shown in (d). (e)–(h) Simulated remanent magnetization states of the top, middle, and bottom layers in the  $xy$  plane for the  $t = 20$ ,  $50$ ,  $100$ , and  $250$  nm films, respectively, with the panels at the bottom showing the corresponding normalized in-plane magnetization components  $m_x$  and  $m_y$  as a function of the  $z$ -position.

The top and bottom layers each contain a region in the center with a net axial magnetization component and regions at the ends of the long axis where the spins cant in order to minimize the magnetostatic energy. Furthermore, the  $t = 250$  nm system with  $\phi = 90^\circ$  is the only NM that exhibits an asymmetrical evolution of  $m_x$  and  $m_y$  as a function of the  $z$ -position, as seen in the bottom panel of Fig. 4(h).

It is interesting to note that in all cases, the experimental results show that at low fields, the magnetization reversal has a significant component of in-plane magnetization compared to the micromagnetic simulations. VSM measurements were also undertaken with the field applied OOP, and the results are shown in Fig. 5(a). All of the films display hysteretic behavior with saturation fields similar to those measured with the field applied along the  $\phi = 90^\circ$  direction, indicating an out-of-plane component of anisotropy that is not taken into account in the micromagnetic simulations. Thin-film x-ray diffraction (XRD) was performed on a series of unpatterned Py films that were fabricated during the same deposition process as the patterned NM arrays. A dominant peak in the XRD spectra was observed for NiFe (111), which indicates that the [111] crystallographic texture is OOP, and while it is known that the Py composition  $\text{Ni}_{81}\text{Fe}_{19}$  has a f.c.c. crystal structure and the magnetostriction coefficient along the [111] direction is negligible, the magnetocrystalline anisotropy easy axis along this direction is small but not negligible. It is therefore possible that the films have grown in such a way that [111] crystallites have grown during the deposition, which combined with an OOP magnetic anisotropy, modifies the magnetization reversal, and could account for the low field magnetization behavior. A dominant OOP anisotropy has been detailed in previous works for Py films with thicknesses exceeding  $250$  nm.<sup>24</sup> This anisotropy was not taken into account when modeling the micromagnetics and may explain some of the discrepancies between the simulations and experimental results. The possibility of including a simple uniaxial anisotropy is discussed in the [supplementary material](#). We do not have a deep understanding of the underlying physics behind the OOP anisotropy, which will require a significant amount of extra study beyond the scope of this short letter.

In this work, we have examined the role that the film thickness plays in determining the magnetization reversal behavior and spin textures in elliptical nanomagnets. It was found using micromagnetic simulations that for thicknesses of  $50$  nm and below, the spin texture of the nanomagnets is uniform throughout the film thickness and is essentially two-dimensional. Increasing the film thickness to  $100$  nm and beyond results in complex spin textures, which are non-uniform through the film thickness with the magnetization increasingly having out-of-plane contributions resulting in the nanomagnets behaving as three-dimensional magnetic structures. The microstructure developed

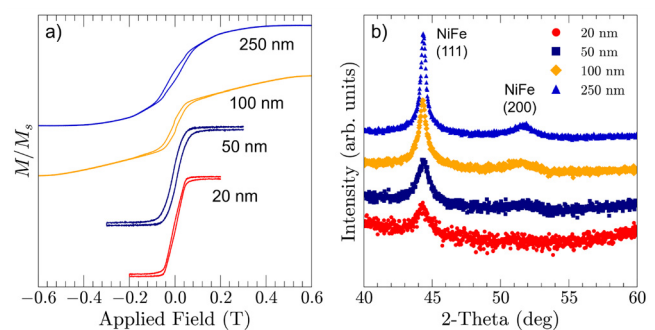


**FIG. 5.** (a) VSM measurements performed on the series of film thicknesses from  $t = 20$  nm to  $t = 250$  nm with the field applied in the out-of-plane (OOP) direction. (b) XRD scans performed on a series of unpatterned continuous films deposited at the same time as each of the patterned arrays.

during film growth appears to influence the reversal behavior and requires further study.

See the [supplementary material](#) for micromagnetic simulations where the magnetostatic interactions between neighboring elements are included as well as simulations where a simple uniaxial OOP anisotropy is incorporated into the micromagnetic model.

The authors thank Dr. Navab Singh for the DUV templates. Dr. William Frost, Dr. David Lloyd, and Professor Atsufumi Hirohata are acknowledged for their assistance with the VSM measurements performed at the University of York. The authors also thank Julius de Rojas for helpful discussions during the development of this research. SEM imaging of the patterned structures was performed at the GJ Russell Electron Microscopy Facility, and XRD was supported by Ben Nicholson. Micromagnetic simulations were performed using Durham University's NCC cluster. A.O.A. would like to thank the Royal Society Wolfson Fellowship. J.R.S. acknowledges support from the Royal Society Studentship.

## AUTHOR DECLARATIONS

### Conflict of Interest

The authors have no conflicts to disclose.

### Author Contributions

**J. R. Scott:** Data curation (lead); Formal analysis (equal); Software (lead); Visualization (equal); Writing – original draft (equal); Writing – review & editing (equal). **D. Atkinson:** Formal analysis (equal); Supervision (equal); Visualization (equal); Writing – original draft (equal); Writing – review & editing (equal). **A. O. Adeyeye:** Conceptualization (lead); Formal analysis (equal); Funding acquisition (lead); Supervision (equal); Visualization (equal); Writing – original draft (equal); Writing – review & editing (equal).

### DATA AVAILABILITY

The data that support the findings of this study are available from the corresponding authors upon reasonable request.

## REFERENCES

- D. A. Allwood, G. Xiong, C. Faulkner, D. Atkinson, D. Petit, and R. Cowburn, "Magnetic domain-wall logic," *Science* **309**, 1688–1692 (2005).
- S. S. Parkin, M. Hayashi, and L. Thomas, "Magnetic domain-wall racetrack memory," *Science* **320**, 190–194 (2008).
- J. W. Lau and J. M. Shaw, "Magnetic nanostructures for advanced technologies: Fabrication, metrology and challenges," *J. Phys. D: Appl. Phys.* **44**, 303001 (2011).
- Z. Luo, A. Hrabec, T. P. Dao, G. Sala, S. Finizio, J. Feng, S. Mayr, J. Raabe, P. Gambardella, and L. J. Heyderman, "Current-driven magnetic domain-wall logic," *Nature* **579**, 214–218 (2020).
- A. Mahmoud, F. Ciubotaru, F. Vanderveken, A. V. Chumak, S. Hamdioui, C. Adelmann, and S. Cotofana, "Introduction to spin wave computing," *J. Appl. Phys.* **128**, 161101 (2020).
- A. Barman, G. Gubbiotti, S. Ladak, A. O. Adeyeye, M. Krawczyk, J. Gräfe, C. Adelmann, S. Cotofana, A. Naeemi, V. I. Vasyuchka *et al.*, "The 2021 magnonics roadmap," *J. Phys.: Condens. Matter* **33**, 413001 (2021).
- R. V. Ababei, M. O. Ellis, I. T. Vidamour, D. S. Devadasan, D. A. Allwood, E. Vasilaki, and T. J. Hayward, "Neuromorphic computation with a single magnetic domain wall," *Sci. Rep.* **11**, 15587 (2021).
- R. P. Cowburn, D. Koltsov, A. Adeyeye, M. Welland, and D. Tricker, "Single-domain circular nanomagnets," *Phys. Rev. Lett.* **83**, 1042 (1999).
- Y. Nakatani, A. Thiaville, and J. Miltat, "Head-to-head domain walls in soft nano-strips: A refined phase diagram," *J. Magn. Magn. Mater.* **290–291**, 750–753 (2005).
- T. Shinjo, T. Okuno, R. Hassdorf, K. Shigeto, and T. Ono, "Magnetic vortex core observation in circular dots of permalloy," *Science* **289**, 930–932 (2000).
- S.-B. Choe, Y. Acremann, A. Scholl, A. Bauer, A. Doran, J. Stöhr, and H. A. Padmore, "Vortex core-driven magnetization dynamics," *Science* **304**, 420–422 (2004).
- B. Van Waeyenberge, A. Puzic, H. Stoll, K. Chou, T. Tylliszczak, R. Hertel, M. Fähnle, H. Brückl, K. Rott, G. Reiss *et al.*, "Magnetic vortex core reversal by excitation with short bursts of an alternating field," *Nature* **444**, 461–464 (2006).
- T. Ono, H. Miyajima, K. Shigeto, K. Mibu, N. Hosoi, and T. Shinjo, "Propagation of a magnetic domain wall in a submicrometer magnetic wire," *Science* **284**, 468–470 (1999).
- D. Atkinson, D. A. Allwood, G. Xiong, M. D. Cooke, C. C. Faulkner, and R. P. Cowburn, "Magnetic domain-wall dynamics in a submicrometre ferromagnetic structure," *Nat. Mater.* **2**, 85–87 (2003).
- G. S. Beach, C. Nistor, C. Knutson, M. Tsoi, and J. L. Erskine, "Dynamics of field-driven domain-wall propagation in ferromagnetic nanowires," *Nat. Mater.* **4**, 741–744 (2005).
- A. Thiaville, Y. Nakatani, J. Miltat, and Y. Suzuki, "Micromagnetic understanding of current-driven domain wall motion in patterned nanowires," *Europhys. Lett.* **69**, 990 (2005).
- J. Ding, G. N. Kakazei, X. M. Liu, K. Y. Guslienko, and A. O. Adeyeye, "Intensity inversion of vortex gyrotropic modes in thick ferromagnetic nanodots," *Appl. Phys. Lett.* **104**, 192405 (2014).
- A. Fernández-Pacheco, R. Streubel, O. Fruchart, R. Hertel, P. Fischer, and R. P. Cowburn, "Three-dimensional nanomagnetism," *Nat. Commun.* **8**, 15756 (2017).
- C. Donnelly, M. Guizar-Sicairos, V. Scagnoli, S. Gliga, M. Holler, J. Raabe, and L. J. Heyderman, "Three-dimensional magnetization structures revealed with x-ray vector nanotomography," *Nature* **547**, 328–331 (2017).
- S. Sahoo, A. May, A. van Den Berg, A. K. Mondal, S. Ladak, and A. Barman, "Observation of coherent spin waves in a three-dimensional artificial spin ice structure," *Nano Lett.* **21**, 4629–4635 (2021).
- D. Sanz-Hernández, C. Donnelly, L. Pérez, and A. Fernández-Pacheco, "Nanofabrication of three-dimensional magnetic structures," in *Nanofabrication: Nanolithography Techniques and Their Applications* (IOP Publishing Bristol, UK, 2020), pp. 11–1–11–38.
- A. O. Adeyeye and N. Singh, "Large area patterned magnetic nanostructures," *J. Phys. D: Appl. Phys.* **41**, 153001 (2008).
- A. Vansteenkiste and B. Van de Wiele, "Mumax: A new high-performance micromagnetic simulation tool," *J. Magn. Magn. Mater.* **323**, 2585–2591 (2011).
- J. Ben Youssef, N. Vukadinovic, D. Billet, and M. Labrune, "Thickness-dependent magnetic excitations in permalloy films with nonuniform magnetization," *Phys. Rev. B* **69**, 174402 (2004).